J. PHYS. IV FRANCE 7 (1997)
Colloque C5, Supplément au Journal de Physique III de novembre 1997

Lattice Dynamics of Martensitic Transformations Examined by Atomistic Simulations

R. Meyer and P. Entel

Theoretische Tieftemperaturphysik, Gerhard-Mercator-Universität, Gesamthochschule Duisburg
Lotharstrasse 1, 47048 Duisburg, Germany

Abstract: We have performed molecular dynamics simulations of $Fe_{80}Ni_{20}$ alloys using an inter-atomic potential of the EAM-type which allows the simulation of the martensite-austenite transition. We present results, showing the development of an inhomogeneous shear system on a nanoscale during the thermally induced austenitic transformation. In addition to this we obtained the phonon dispersion relations of the martensite phase by calculating the dynamical structure factor from our simulation results. On approaching the transition temperature the phonon dispersion shows anomalies which might be connected with the formation of the microstructure during the austenitic transition.

1. INTRODUCTION

Relationships between atomistic processes and the formation of the microstructure during martensitic transformations are not well understood today. In order to get more insight into this we have performed molecular dynamics simulations of Fe_xNi_{1-x} alloys. Within the range $0.66 < x < 1.0$, these alloys show experimentally a martensitic transformation from a fcc high-temperature phase to a low-temperature bcc phase (see for example [1] and references therein).

Most investigations in the context of martensitic transformations concentrate on the austenite to martensite transition. This is reasonable since the formation of microstructure during the martensitic transformation influences the properties of the low-temperature phase to a high degree and makes it rather difficult to investigate the features of the homogeneous martensitic phase. Nevertheless it is desirable to study the homogeneous phase, in order to be able to distinguish between genuine features of the martensitic phase and those caused by the microstructure. Therefore, we have done simulations in the low-temperature bcc phase, looking for the processes leading to the austenitic transition which also lead to the formation of a microstructure in the high-temperature phase.

We present results of two distinct simulation sequences. We begin with a study of the formation of a microstructure on a nanometer lengthscale. These simulations required the consideration of a large number of atoms. In order to do this we employed a semi-empirical potential which is based on the embedded-atom method (EAM) introduced by Daw and Baskes [2, 3]. This enabled us to simulate systems with characteristic linear dimension larger than 5 nm. Despite of the fact that this is, physically spoken, still a small system, we find the formation of a microstructure with an inhomogeneous shear system.

In a second investigation we calculated the phonon dispersion curves of $Fe_{80}Ni_{20}$ in the bcc phase. Our results show that the austenitic transition of $Fe_{80}Ni_{20}$ is accompanied by similar phonon anomalies as those observed in many martensitic transformations [4]. We find two anomalies which we believe to be related to the structural transition and the specific form of the microstructure. Though pure iron also exhibits the martensitic transformation, we demonstrate how the addition of Ni destabilizes the bcc structure.

2. COMPUTATIONAL METHODS

Classical molecular dynamics simulations have been performed, using a semi-empirical potential based on the EAM which has been constructed recently for the study of martensitic transformations in Fe_xNi_{1-x} alloys [5, 6]. In contrast to simple pair-potentials, potentials based on the EAM are able to describe the elastic behaviour of a metal correctly, while remaining computationally efficient.

Standard techniques of molecular dynamics simulations [7] like periodic boundary conditions and the Verlet algorithm for the integrations of the equations of motion with a time step $\delta t = 1.5 \times 10^{-15} s$ have been employed. Both simulation sequences started with configurations of atoms on an ideal bcc lattice with a random distribution of Fe and Ni atoms.

The first simulation sequence was done with a configuration of 16000 atoms ($20 \times 20 \times 20$ cubic bcc elementary cells) having an iron concentration $x = 80.01$ %. This system was heated from a temperature of $T = 600$ K to 700 K in steps of 50 K. Afterwards the temperature was increased in steps of 20 K until the austenitic transformation occurred at $T = 860$ K. At each temperature 1000 simulation steps were done in order to reach thermal equilibrium and another 10000 steps (15 ps) for measurement purposes. These simulations were carried out within the isothermal-isobaric ensemble generated by the Nosé-Hoover thermostat [8, 9] and the Parrinello-Rahman scheme [10, 11] with a fluctuating simulation box.

The second set of simulations used a smaller configuration of $12 \times 12 \times 12$ cubic elementary cells (3456 atoms) with the same iron concentration $x = 80.01\%$. This system was simulated at temperatures T = 300, 500 and 700 K with a fixed simulation box and within the microcanonical ensemble. From a previous investigation the equilibrium lattice parameters were known. After the equilibration phase 40000 simulation steps (60 ps) were done, writing the atomic positions to a file after every 10th simulation step. From this file the dynamic structure factor [12]

$$S(\mathbf{q},\omega) = \frac{1}{N} \sum_{\mathbf{R},\mathbf{R}'} e^{-i\mathbf{q}\cdot(\mathbf{R}-\mathbf{R}')} \int \frac{dt}{2\pi} e^{i\omega t} \langle \exp[i\mathbf{q}\cdot\mathbf{u}(\mathbf{R}',0)] \exp[-i\mathbf{q}\cdot\mathbf{u}(\mathbf{R},t)] \rangle \qquad (1)$$

has been calculated (N is the number of atoms and $\mathbf{u}(\mathbf{R},t)$ represents the displacement of the atom from the ideal lattice position $\mathbf{R}$ at time t). The phonon dispersion curves were obtained by evaluating the positions of the peaks of $S(\mathbf{q},\omega)$ at different wave-vectors $\mathbf{q}$.

3. RESULTS

3.1 Microstructure formation

The simulations done with 16000 atoms revealed the same general characteristics of the martensitic phase and the austenitic transition as similar calculations of smaller systems did[5, 6]. In particular identical structural and orientational relationships were observed. One of the $(110)_{bcc}$ plane sets changed to a set of close packed planes, remaining the [001] direction parallel to this planes unrotated. However, more interesting is the structure of the resulting austenite phase. Figure 1 shows two atomic layers of the resulting structure viewed along the unrotated [001] direction. The stacking sequence of the close packed planes turns out to be *ABCABCACABABCABCBCAC* (from left to right). Keeping in mind the periodic boundary conditions, it can be seen from the stacking sequence and Fig. 1 that the whole system consists of two big fcc plates (6 and 8 layers thick) which are separated by thin 3 layer plates. The slip faults which separate these basic blocks lead to an inhomogeneous shear angle of 2.5°. The atomic movements that generated the structure of the system in Fig. 1 are elucidated by Fig. 2, which displays the deviations of the atoms drawn in Fig. 1 from ideal body-centered lattice positions. Comparing Fig. 1 and Fig. 2 one can see that the areas with a regular stacking sequence are formed by a homogenous shear of the $(110)_{bcc}$ planes along the $[1\bar{1}0]_{bcc}$ direction. At the slip boundaries between the homogenous regions the displacement field reverts its direction which leads to abrupt jumps.

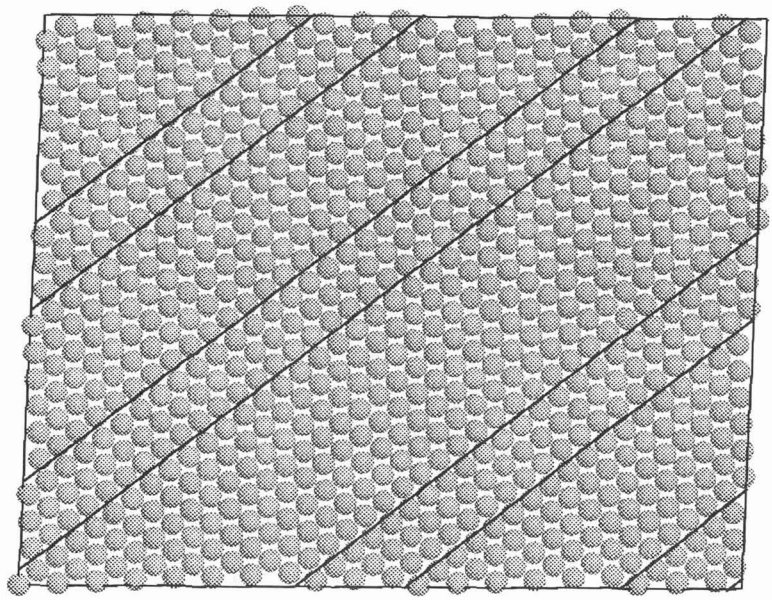

Figure 1: Two atomic [001] layers of the simulated $Fe_{80}Ni_{20}$ crystal after the austenitic transformation. The diagonal lines indicate stacking faults of the (111) planes.

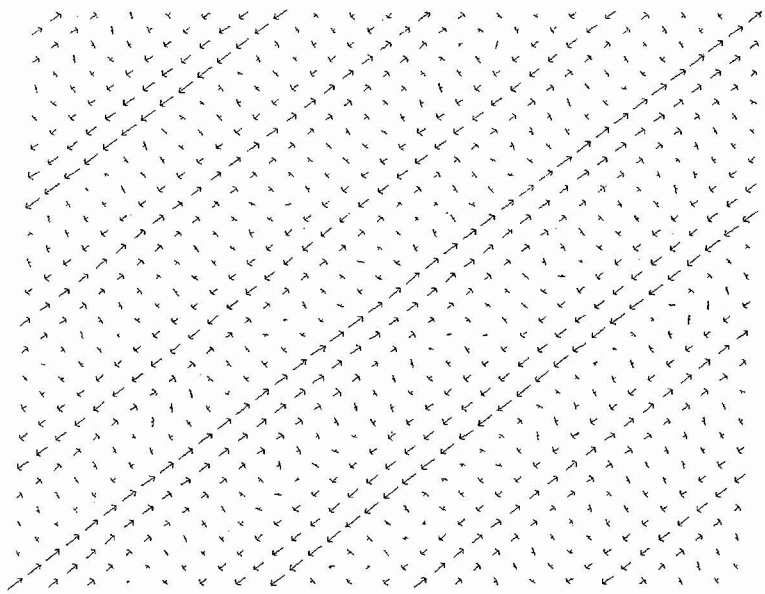

Figure 2: Deviations of the positions of the atoms in Fig. 1 from an ideal body-centered structure. Arrows are enlarged by a factor of 2.

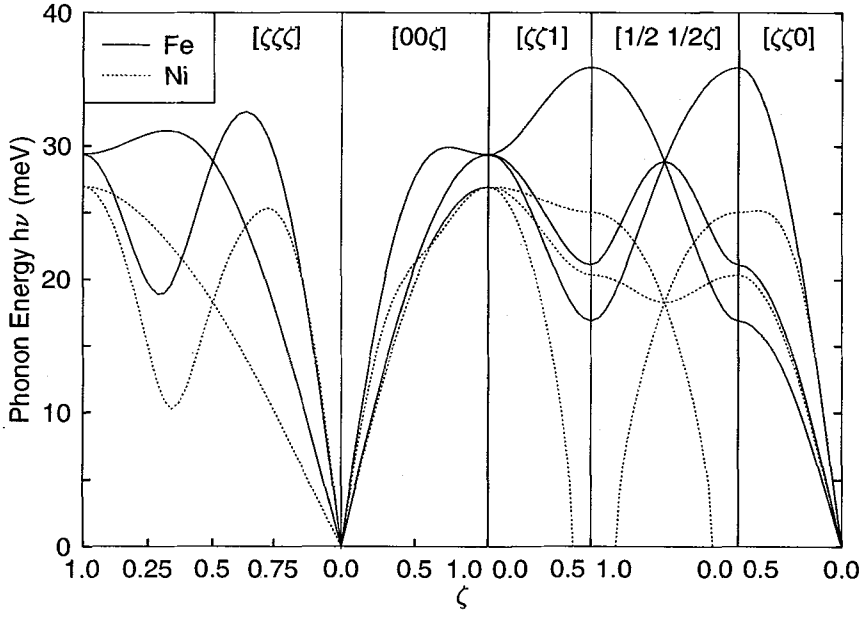

Figure 3: Phonon dispersion curves of bcc Fe and Ni with lattice constant $a_0 = 5.4369\, a_B$. The spectra have been calculated analytically from the EAM-potentials.

3.2 Phonon dispersion relations

In order to see the effects of alloying on the phonon dispersion curves, first the phonon spectra of pure Fe and Ni were calculated analytically from the EAM-potentials by diagonalization of the dynamical matrix. Figure 3 shows the result, obtained for a bcc structure with lattice constant $a_0 = 5.4369\, a_B$ determined for $Fe_{80}Ni_{20}$ at $T = 300$ K from the simulations. Along the $\mathbf{q} = [111]$ and [001] directions both elements show a normal behaviour. Along the other directions considered in Fig. 3 this is only true for Fe. Around $\mathbf{q} = [\frac{1}{2}\frac{1}{2}1]$ and along the $\mathbf{q} = [110]$ direction the spectrum of Ni exhibits a strange behaviour and one of the modes has negative squares of frequencies here. This result itself is not very exceptional since experimentally Ni shows no stable bcc phase. But the unstable mode along the [110] direction corresponds in the limit $\mathbf{q} \to \mathbf{0}$ to a negative elastic constant $C' = \frac{1}{2}(C_{11} - C_{12})$. This is consistent with *ab initio* electronic structure calculations which also reveal a negative value of C' [13].

With respect to this instability of Ni and the fact that the bcc - fcc transition requires a shear along $[110]_{bcc}$, this direction appears to be a good candidate for phonon anomalies in those Fe_xNi_{1-x} alloys, which exhibit a martensitic transformation. Figure 4 shows the phonon dispersion curves of $Fe_{80}Ni_{20}$ along this direction determined from molecular dynamics simulations by calculation of the dynamic structure factor $S(\mathbf{q}, \omega)$ at $T = 300$ K (a), and the temperature dependence of the low lying TA_2 mode (b). The data points in these figures represent the positions of the peaks in $S(\mathbf{q}, \omega)$ averaged over all crystallographically equivalent [110] directions. The error bars are derived from the corresponding standard deviations. If no error bars are drawn, the standard deviations are smaller than the symbol sizes.

Figure 4(a) demonstrates the dramatic effect of Ni on the phonon dispersion curves. The longitudinal and the upper transversal modes are shifted to higher frequencies, while the energies of the low lying transversal branch are reduced by almost a factor 2. At $\mathbf{q} = \frac{1}{3}[110]$ a small dip in the longitudinal branch occurs. But the values at this wave vector also have the largest errors. Therefore, it is difficult to decide wether this dip together with the errors represent physics or not. In contrast

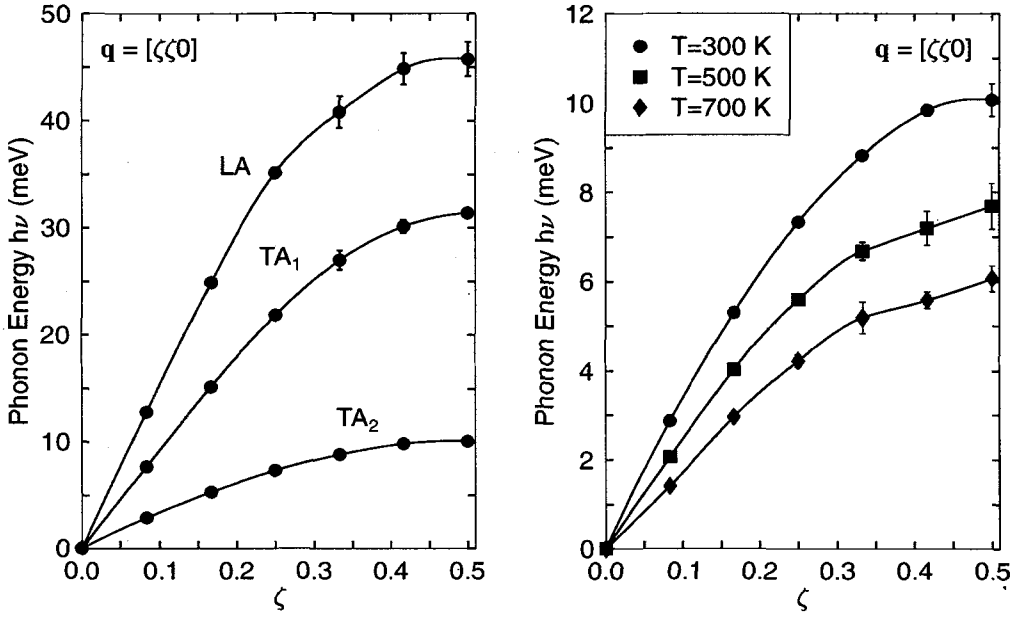

Figure 4: (a) Phonon dispersion curves of $Fe_{80}Ni_{20}$ in the bcc phase along [110], as determined from the simulation at 300 K. (b) Temperature dependence of the TA_2 mode (polarization along $[1\bar{1}0]$) along the [110] direction.

to this in Fig. 4(b) it can be seen without doubts that the low lying transversal mode develops two distinct anomalies on approaching the transition temperature. At $\mathbf{q} \rightarrow \mathbf{0}$ the slope of the branch reduces with increasing temperature, leading to a positive curvature of the corresponding dispersion relation. The second anomaly is located between $\mathbf{q} = \frac{1}{3}[110]$ and the Brillouin-zone boundary. The dip occurring here in the transversal mode is also accompanied by large errors of the data points.

4. DISCUSSION AND CONCLUSIONS

Results of molecular dynamics simulations shown in Fig. 1 and Fig. 2 demonstrate the formation of an inhomogeneous shear system during the austenitic bcc - fcc transition in Fe_xNi_{1-x} alloys. This shear system is quite similar to that observed in the austenite martensite - transitions of these systems. The microstructure consists of homogeneous fcc plates separated by slip faults. Though the length scale of these simulations is still far too small to give definite answers, it is interesting to see that the thicker fcc plates are separated by rather thin plates consisting of only three atomic layers. This could be just a random result of this particular simulation. But this observation is confirmed by the anomalies of the phonon dispersion curves resulting from the second simulation sequence, since wavelength and direction of the anomaly between $\mathbf{q} = \frac{1}{3}[110]$ and the zone boundary are in accordance with the microstructure observed in Fig. 1. Therefore we think that the formation of the microstructure during the transformation can be attributed to this anomaly which is visible at temperatures far below the actual transformation. Nevertheless, simulations of even larger systems have to be done to assure that the structures we find are not artefacts of finite-size effects.

The other anomaly at $\mathbf{q} \rightarrow \mathbf{0}$, in the phonon dispersion curves leads to a low value of the elastic constant C', which probably vanishes near the transition temperature. This is the driving force behind the austenitic transformation itself and has probably no further effect on the microstructure.

From Fig. 4(a) the effects of the addition of Nickel on the phonon dispersion curves can be seen. The most striking effect is the reduction of the low-temperature value of C'. This explains the decrease of the austenitic transition temperatures with increasing Ni contents [1].

It is clear that under normal experimental conditions, the properties of the martensitic phase are dominated by the microstructure which develops during the martensitic transformation. But we think that the results of our present molecular dynamics simulations show that the austenitic transition also has its own genuine features which are worth to be studied. To our knowledge there are no experimental data of the phonon dispersion relations of the bcc phase of Fe_xNi_{1-x} available at the time being. It will be very interesting to see if our theoretical prediction can be confirmed experimentally.

Acknowledgments

This work has been supported by the *Deutsche Forschungsgemeinschaft* (DFG) within the *Sonderforschungsbereich* SFB 166. We also want to thank the *Höchstleistungsrechenzentrum* HLRZ Jülich, Germany, for the CPU-time on its Intel Paragon. Parts of our calculations have been done there.

References

[1] Acet M., Schneider T. and Wassermann E.F., "Magnetic aspects of Martensitic Transformations in FeNi Alloys", IV European Symposium on Martensitic Transformations, Barcelona 1994, A. Planes, J. Ortín and Ll. Mañosa Eds. (Les editions de physique, 1995) pp. 105-109.

[2] Daw M.S. and Baskes M.I., *Phys. Rev. Lett* **50** (1983) 1285-1288.

[3] Daw M.S. and Baskes M.I., *Phys. Rev. B* **29** (1984) 6443-6453.

[4] Delaey L., Diffusionless transformations, in: *Phase Transformations in Materials*, Materials Science and Technology, Volume **5**, R. W. Cahn, P. Haasen, and E. J. Kramer, eds., VCH, Weinheim (1972).

[5] Meyer R., Kadau K. and Entel P., "The Martensitic Transformation in Iron-Nickel Alloys: A Molecular Dynamics Study", 1. International Alloy Conference, Athens 1996, (Plenum) in press.

[6] Meyer R., Entel P., "Molecular Dynamics Study of Iron-Nickel Alloys", IV European Symposium on Martensitic Transformations, Barcelona 1994, A. Planes, J. Ortín and Ll. Mañosa Eds. (Les editions de physique, 1995) pp. 123-128.

[7] Allen M.P., Tildesley D.J., Computer Simulations of Liquids (Clarendon, Oxford, 1987).

[8] Nosé S., *Mol. Phys.* **52** (1984) 255-268.

[9] Hoover W.G., *Phys. Rev. A* **31** (1985) 1695-1697.

[10] Parrinello M., Rahman A., *Phys. Rev. Lett.* **45** (1980) 1196-1199.

[11] Parrinello M., Rahman A., *J. Appl. Phys.* **52** (1981) 7182-7190.

[12] Ashcroft N.W., Mermin N.D., Solid State Physics, (Holt, Rinehart and Winston, New York, 1976), p. 792.

[13] Egbert Hoffmann, private communication.